JGR Space Physics

RESEARCH ARTICLE
10.1029/2020JA027794

Determining the Nominal Thickness and Variability of the Magnetodisc Current Sheet at Saturn

N. R. Staniland[1], **M. K. Dougherty**[1], **A. Masters**[1], **and E. J. Bunce**[2]

[1]Blackett Laboratory, Imperial College London, London, UK, [2]Department of Physics and Astronomy, University of Leicester, Leicester, UK

Key Points:
- The median current sheet half-thickness is 1.3 Saturn radii, but spatial and temporal variability is identified
- The current sheet is 50% thicker on the nightside close to the planet but reduces more significantly with radial distance than the dayside
- The planetary period modulations organize some of the variability, but there is evidence of other temporal drivers

Supporting Information:
- Supporting Information S1
- Table S1

Correspondence to:
N. R. Staniland,
n.staniland17@imperial.ac.uk

Citation:
Staniland, N. R., Dougherty, M. K., Masters, A., & Bunce, E. J. (2020). Determining the nominal thickness and variability of the magnetodisc current sheet at Saturn. *Journal of Geophysical Research: Space Physics*, *125*, e2020JA027794. https://doi.org/10.1029/2020JA027794

Received 10 JAN 2020
Accepted 8 APR 2020
Accepted article online 16 APR 2020

Abstract The thickness and variability of the Saturnian magnetodisc current sheet is investigated using the Cassini magnetometer data set. Cassini performed 66 fast, steep crossings of the equatorial current sheet where a clear signature in the magnetic field data allowed for a direct determination of its thickness and the offset of its center. The average, or nominal, current sheet half-thickness is 1.3 R_S, where R_S is the equatorial radius of Saturn, equal to 60,268 km. This is thinner than previously calculated, but both spatial and temporal dependencies are identified. The current sheet is thicker and more variable by a factor ~2 on the nightside compared to the dayside, ranging from 0.5–3 R_S. The current sheet is on average 50% thicker in the nightside quasi-dipolar region (≤15 R_S) compared to the dayside. These results are consistent with the presence of a noon-midnight electric field at Saturn that produces a hotter plasma population on the nightside compared to the dayside. It is also shown that the current sheet becomes significantly thinner in the outer region of the nightside, while staying approximately constant with radial distance on the dayside, reflecting the dayside compression of the magnetosphere by the solar wind. Some of the variability is well characterized by the planetary period oscillations (PPOs). However, we also find evidence for non-PPO drivers of variability.

Plain Language Summary A key discovery of the Cassini orbital mission at Saturn was that the small moon Enceladus was geologically active. Water from a subsurface ocean escapes as vapor through geysers in the moon's southern hemisphere. A significant portion becomes ionized and interacts with the magnetic environment that surrounds Saturn, called its magnetosphere. Due to the rapid rotation rate of the planet, this layer of charged particles sourced from Enceladus is stretched into a thin disc around Saturn, known as the magnetodisc current sheet. In this study, we explore the thickness of the current sheet, identifying its average structure and potential sources of variability. We find that the current sheet thickness depends on both the distance from Saturn and position in local time with respect to the Sun. We also find that some of the variability about its average state is somewhat described by the presence of a magnetic perturbation system that occurs close to the rotation period of Saturn. These results are essential for accurately modeling the magnetosphere of Saturn and understanding how the system responds to different drivers of variability.

1. Introduction

The presence of an equatorial current sheet shapes the global magnetic field structure of Saturn. This current system, known as the magnetodisc current sheet, is internally sourced, predominantly by the moon Enceladus (Dougherty et al., 2006) which orbits at 3.95 R_S, where R_S = 60,268 km is the equatorial radius of Saturn. Water vapor is emitted from geysers in the southern hemisphere of the moon at a rate of ~70–750 kg/s (Bagenal & Delamere, 2011). A portion of these water group neutrals become ionized through electron impact ionization and photoionization, locking onto the magnetic field lines and are accelerated toward corotation due to field-aligned currents transferring angular momentum from the ionosphere to the plasma. Due to the fast ~10.6 hr rotation rate of Saturn, the plasma is centrifugally confined to the equator, radially stretching the dipolar field outward into the characteristic "magnetodisc" geometry. Hence, the azimuthal current flowing in the equatorial sheet is a sign of the force balance in the magnetodisc. The current sheet has been observed at all local times, reaching the magnetopause on the dayside and merging with the magnetotail plasma/current sheet that separates the two lobes on the nightside. While the equatorial current

sheet is often referred to as the ring current, with reference to the terrestrial system, since Saturn is rotationally dominated and this plasma is internally sourced, we instead refer to it as the magnetodisc current sheet, or simply the current sheet.

The magnetodisc geometry that the current sheet supports was not initially identified at Saturn in the magnetometer data of the early flyby missions, except at dawn (Smith et al., 1980), implying the current sheet was too weak to distort the field entirely. However, Arridge et al. (2008) showed using the Cassini magnetometer data (Dougherty et al., 2004) that this phenomena is observed at all local times under expanded magnetospheric conditions. This can occur due to both the external and internal sources, such as the solar wind, increased suprathermal plasma pressure (Pilkington et al., 2015) related to Vasyliunas-type reconnection (Vasyliunas, 1983), and variable outgassing of Enceladus (Smith et al., 2010) that could increase the plasma content of the current sheet. Therefore, the large-scale properties of the current sheet are expected to have both spatial and temporal dependencies that will reflect these changes in the global configuration.

The radial extent and total current flowing through the current sheet varies with system size, increasing when the magnetosphere is expanded and reducing when the system is compressed (Bunce et al., 2007, 2008). Staniland et al. (2018) tracked the strength of the current sheet throughout the Cassini mission and identified a local time asymmetry, revealing the field to be more compressed at dusk than dawn. Empirical models and simulations have also identified this asymmetry, showing a 5–10% difference in the location of the magnetopause at dawn and dusk (Jia & Kivelson, 2016; Pilkington et al., 2015; Sorba et al., 2019). On average, for radial distances greater than >15 R_S, a region defined as the magnetodisc-proper (Arridge et al., 2008), the magnetic field becomes predominantly radial and the current sheet determines the field geometry. At smaller radial distances, the stronger internal magnetic field determines the field geometry and so it appears quasi-dipolar in configuration.

The thickness of the magnetodisc current sheet is also expected to be modified in response to changes in the system configuration. The thickness was initially calculated from flybys of Saturn by the Pioneer and Voyager spacecraft and was found to have a half-thickness of ∼2.5 R_S (Bunce & Cowley, 2003; Connerney et al., 1981b; Giampieri & Dougherty, 2004). This value was obtained by fitting the Connerney et al. (1981a) model to the Voyager and Pioneer data. However, these spacecraft did not pass through both the northern and southern boundaries of the current sheet, and so the thickness was not uniquely determined. Kellett et al. (2009) calculated the thickness directly by using six steep crossings of the current sheet made by Cassini in 2006 and 2007. They found that the half-thickness varied between 0.4 and 2 R_S, being thickest in the middle magnetosphere (9–15 R_S) and thinnest in the outer magnetosphere (>15 R_S) on both the dayside and the nightside. However, this study was performed early in the mission when there was a limited understanding of the temporal variability of the current sheet and so these features were attributed to a spatial dependence.

Sergis et al. (2011) determined the thickness of the magnetotail current sheet by fitting a Harris current sheet (Harris, 1962) to four steep crossings made by Cassini in 2007 and 2009. They identified a thin current sheet, embedded within a thicker plasma sheet, where the thickness varied with different energies of particle populations. This was understood in terms of the centrifugal scale height $\propto (k_B T/m)^{\frac{1}{2}}$ for a population of particles with temperature $k_B T$, where k_B is the Boltzmann constant and m is the particle mass (Hill & Michel, 1976). This implies that the heavier, colder, ions would be constrained to the equator, whereas the hotter and more energetic plasma populations will be distributed further along the magnetic field lines. The focus of this study will be on the current sheet rather than the plasma sheet, and this can be identified using only the magnetic field data.

A significant source of temporal variability in the current sheet thickness are the planetary period oscillations (PPOs). These have been observed in almost all magnetospheric observations (see review by Carbary & Mitchell, 2013, and references therein) and are one of the key drivers of large-scale dynamics within the Saturnian magnetophere. It is argued that the presence of two rotating vortices in the polar regions of Saturn's thermosphere (Jia et al., 2012; Smith, 2006) drive perturbations upward into the magnetic field, generating hemispheric field-aligned current systems that rotate with the planet. Using magnetic field and Saturn Kilometric Radiation (SKR) data, the periods of these two systems have been determined for the complete Cassini mission (Andrews et al., 2008, 2012; Cowley & Provan, 2015, 2016; Gurnett et al., 2009, 2011; Kurth et al., 2007, 2008; Lamy, 2011, 2017; Provan et al., 2013, 2014, 2016, 2019) and shown to each have separate and varying periods, close to ∼10.6 hr (Hunt et al., 2014, 2015, 2016; Southwood & Kivelson, 2007; Southwood & Cowley, 2014). The resultant perturbation magnetic fields due to these currents are

quasi-uniform across the equator and quasi-dipolar in each hemisphere, closing over the respective poles. These perturbation fields affect the background magnetic field, producing both radial and meridional modulations that are characterized by $\Phi_{N,S}$, the azimuthal position with respect to these systems. Variations in the thickness and offset of the current sheet are expected to be functions of the PPO phases, which has been observed in the tail current sheet (Cowley & Provan, 2017; Provan et al., 2012; Thomsen et al., 2017) and subsequently modeled (Agiwal et al., 2020; Arridge et al., 2011; Cowley et al., 2017).

In this study, we will use the complete Cassini orbital magnetometer data set to find when the spacecraft made fast, steep traversals of the magnetodisc current sheet, allowing us to directly determine its thickness. We aim to characterize the results in terms of the most significant sources of spatial and temporal variability within the Saturnian magnetosphere and reveal what this implies for the global structure of the Saturnian system.

2. Data Selection

The complete Cassini orbital magnetometer data set at 1-min resolution is surveyed to find all crossings of the current sheet. Higher-resolution data are not required for identifying the current sheet boundaries. We transform the data into the Kronocentric Solar Magnetic (KSMAG) coordinate system, where the Z axis of the orthogonal system points along the magnetic dipole vector, the X-Z plane contains the Sun vector with X directed sunward, and the Y axis completes the system. For studying the current sheet it is best to work in cylindrical coordinates, assuming that it is not significantly warped, given by (ρ, ϕ, z) where ρ is the perpendicular distance from the Z axis and positive when pointing away from Saturn, and ϕ is the azimuthal angle whereby $\phi = 0$ is equivalent to local time noon and it increases in the direction of planetary rotation. To begin, the Cassini-11 internal magnetic field model (Dougherty et al., 2018) up to degree 4 is subtracted, since higher-degree terms are unnecessary in our region of interest. To identify a current sheet crossing, we look for reversals in B_ρ and a monotonic signature during the reversal, indicating Cassini has passed through a current sheet. However, this signature alone is insufficient for identifying a crossing of the magnetodisc current sheet, and could instead be due to another current layer or some transient event that has modified the local field structure. Therefore, a set of criteria for identifying magnetodisc current sheet crossings must be defined.

The plasma sourced from Enceladus which populates the magnetodisc current sheet is transported radially outward from the moon and eventually lost down tail through plasmoid ejections, which are a consequence of either the rotationally driven Vasyliunas cycle (e.g,. Cowley et al., 2015; Vasyliunas, 1983), the solar wind-driven Dungey cycle (e.g., Dungey, 1961; Thomsen et al., 2015), or the thinning of the current sheet by the PPOs (e.g., Bradley et al., 2018). Therefore we look for crossings that occurred at radial distances greater than 3.95 R_S. Second, we look for crossings close to the dipole magnetic equator, where we expect the current sheet to be situated. However, the seasonal warping of the current sheet (Arridge et al., 2008) implies that we must define a minimum and maximum expected deviation from the dipole magnetic equator. Martin and Arridge (2017) found that current sheet center is most commonly located between $z = \pm 5\ R_S$ and so we set this as our vertical range. The magnetic field strength either side of the crossing is calculated and compared with the statistical lobe magnetic field model of Jackman and Arridge (2011) to ensure we are measuring current sheet crossings and not some other transient event that results in a reversal of B_ρ. A further cross-check with the Jackman et al. (2019) list of magnetopause crossings is required to ensure that the event is indeed a current sheet crossing. Reversals in B_ρ can also be due to Titan flybys and are found often near current sheet crossings. These can be further identified by a reversal in B_ϕ and an enhancement in the electron density and so these events were removed from our analysis. Finally, the current sheet motion is highly dynamic, varying on long time scales due to the seasonal warping and on short time scales due to the PPOs. Therefore Cassini must be traveling at a velocity greater than the expected motion of the current sheet. Agiwal et al. (2020) modeled the nightside current sheet, revealing the motion of the tail current sheet and its variability. From this, we define a minimum vertical speed for Cassini to be $v_z = 5$ km/s. The distribution of Cassini's vertical speed during the orbital mission has two peaks, each associated with the average apoapse and periapse speed. Our chosen v_z threshold removes data collected when Cassini was less than the peak associated with the average apoapse speed. Therefore, crossings where these criteria are fulfilled will be used to directly determine the thickness of the current sheet.

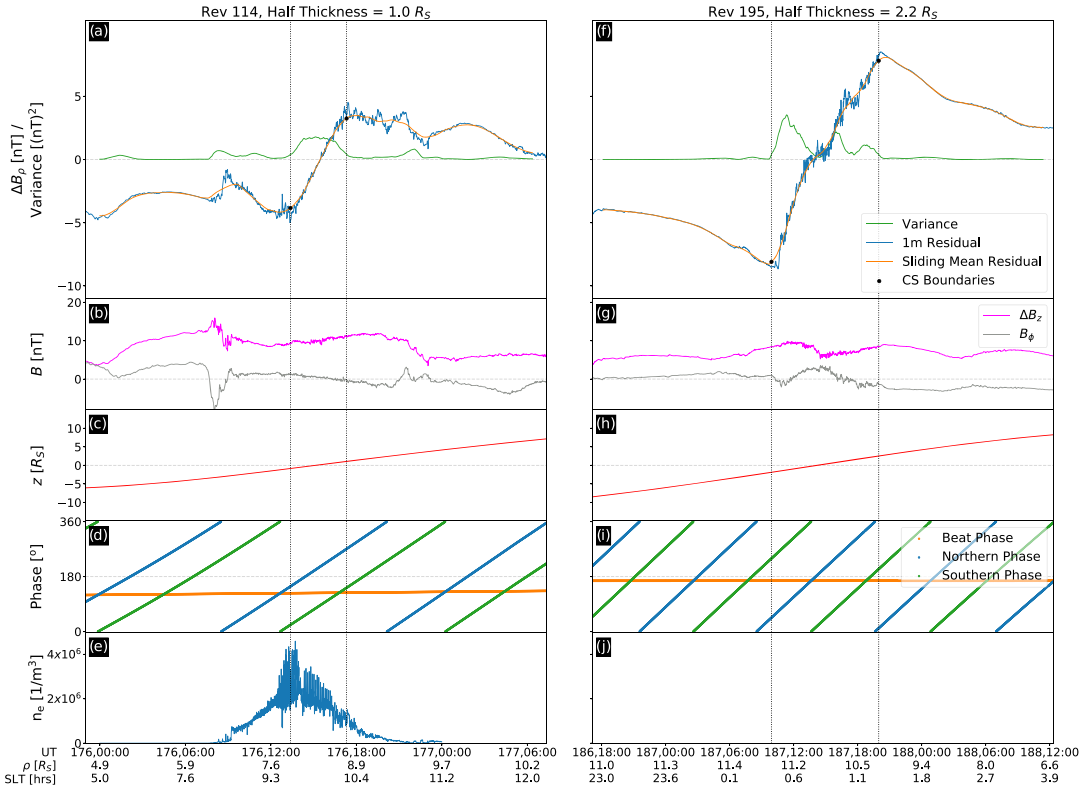

Figure 1. Residual magnetic field data, having subtracted the Dougherty et al. (2018) internal field model, for Rev 114 in 2009 is shown on the left and Rev 195 in 2013 is shown on the right, both as a functions of time. Note that the plotted range of time for Rev 195 is longer than for Rev 114. Panels (a) and (f) show ΔB_ρ at 1-min resolution in blue, with a 2-hr sliding mean shown in orange. The green line shows the variance calculated in the sliding window. A clear spike identifies the current sheet (CS) crossing, with the boundaries shown by the dashed lines. Panels (b) and (g) show ΔB_z and B_ϕ, both of which lack a clear signature of the current sheet boundaries. Panels (c) and (h) show Cassini's distance from the equator in KSMAG coordinates. Panels (d) and (i) show the northern, southern, and beat phases of the PPOs in blue, green, and orange, respectively. Both cases are in near-antiphase conditions. Panel (e) shows the bulk thermal electron density determined using the CAPS ELS instrument for Rev 114. This plot show the density, rather than the density with the penetrating radiation subtracted. Panel (j) is empty because the instrument was turned off in 2012. At the bottom of the figure the day of year and time, the perpendicular distance of Cassini from the dipole axis, and Cassini's local time position in decimal hours are shown.

3. Determining the Thickness

The complete Cassini orbital magnetometer data set at 1-min resolution is surveyed using this set of criteria to find all suitable current sheet crossings. Two examples of these are shown in Figure 1. For each example, there is a clear B_ρ reversal, shown in Figures 1a and 1f, implying that the center of the current sheet has been crossed, with an approximately linear variation in B_ρ as Cassini cuts through the layer of plasma. B_ρ then either remains constant or reduces with height from the current sheet as the field becomes less radial. In Figures 1b and 1g, B_z remains approximately constant due to the zero divergence of the magnetic field. Hence, the boundaries of the current sheet are determined from the signature of B_ρ alone and are shown for the two examples in Figure 1 with dashed vertical lines.

We use a new method for identifying the current sheet boundaries by calculating the variance of B_ρ in a 1-hr sliding window. When B_ρ is steady, the variance is approximately zero. When B_ρ is highly variable, for instance, during a current sheet crossing, there is a significant increase in the variance and so we can use the beginning and end of this increase to identify the boundaries of the current sheet. Based on visual inspection of the data, we define a minimum threshold for this increase to be when the variance is greater than or equal to 0.4 nT^2. Marginally varying this threshold does not significantly alter the chosen location since we are looking for a sudden increase in the variance, so we essentially need to set the limit to be when the variance is not approximately zero. However, based on visual inspection this value was found to best identify the boundaries for all of the events, including those where the spike in the variance was less pronounced. Figures 1a and 1f show that this threshold provides a good estimate for identifying the current sheet boundaries.

For some cases, such as Rev 195 in Figure 1, there are multiple spikes in the variance during a crossing due to the B_ρ signature between the two boundaries not being perfectly linear. To account for this, we assume that if variance falls below 0.4 nT^2 for only a short period (chosen to be less than 45 min based on testing different values on our set of events), or if the field magnitude is less than half the value of the field magntitude at the first boundary (assuming the field will be of a similar magnitude either side of the current sheet), Cassini is determined to still be within the current sheet. The reduction in the variance below the threshold is therefore not due to the spacecraft passing through the boundary. Nonetheless, the location of the current sheet boundary could not always be identified by this method because the variability in B_ρ during a crossing was sometimes too large, most likely due to a faster current sheet motion in these instances. These events were discarded so that only events with a clear signature were used.

This variance analysis is performed multiple times while increasing the sliding window size until the results converge within 2σ of the average position. The z position of Cassini in KSMAG coordinates at the current sheet boundaries is given by z_1 and z_2 and these are used to determine its structure. The half-thickness of the current sheet is given by $|z_2 - z_1|/2$ and the offset of the current sheet centers given by $(z_2 + z_1)/2$, assuming the current sheet is not significantly warped.

The other approach for determining the current sheet boundaries is by using a model, such as the Connerney et al. (1981a) (CAN) model. However this can be slow due to the model formulae being integrals over Bessel functions that must be evaluated numerically. In addition, we are not aiming to give a complete description of the current sheet, nor are we aiming to test the validity of any models. For determining the current sheet boundaries, a data-driven approach using this simple variance analysis of the B_ρ signature is suitable and efficient. Nonetheless, an additional cross-check of our results was performed by using the Edwards et al. (2001) analytic approximations of the CAN model. Using the boundaries identified with the above variance analysis as an initial condition, a nonlinear least squares procedure was used to fit the model to the magnetic field data until a best fit was found and the half-thickness could be determined. The results were not significantly different to our method, and we found the same median half-thickness value and day-night asymmetry that will be discussed in Section 4. This is unsurprising considering the method outlined here was constructed to identify the same field signature as the model. Since these analytic approximations are simplifications of the original model, and are not without error, we will use the results from the variance analysis method presented here. We have identified 66 crossings of the magnetodisc current sheet where we can use the this method to determine its thickness.

An assumption of this method is that the current sheet thickness should be measured parallel to the dipole axis. However, if the current sheet is warped out of the equator, as is expected due to the seasonal displacement of the current sheet (Arridge et al., 2008), the current sheet normal will not be perpendicular to the equator. To test how our measurements would be altered by including this offset, we use Minimum Variance Analysis (MVA) to determine the current sheet normal (Sonnerup & Scheible, 1998). Assuming the current sheet is a thin tangential discontinuity which is not time dependent, the divergence of the magnetic field through the current sheet should be zero and so its normal should have a fixed direction. Hence, the direction of minimum variance during a current sheet crossing should be equivalent to the current sheet normal. To calculate the normal, a sliding average of the magnetic field during a current sheet crossing is taken and MVA is performed. The standard deviation of the calculated normal is found using the bootstrapping method, as described by Kawano and Higuchi (1995). However, MVA is not always conclusive in determining the normal. For instance, if there is variability in B_z of a similar order of magnitude to the variability in B_ϕ, MVA cannot distinguish between the direction of minimum and intermediate variance. In this case, we instead use the Coplanarity Method. This calculates the normal by finding $\Delta B \times \left(B_N \times B_S\right)$, where B_N and B_S are the mean magnetic field calculated at the northern and southern current sheet boundaries, so taking their cross product gives a vector tangential to the sheet, ΔB is the difference between these two vectors and is in the plane of the sheet. Therefore the cross product of these will give a vector perpendicular to the current sheet. Knowing the standard deviation of the mean vectors B_N and B_S, we use error propagation to determine the standard deviation of the normal vector calculated using the Coplanarity Method. When these are smaller than the MVA bootstrap errors, or the MVA eigenvalue analysis was degenerate, the Coplanarity Method is used instead.

Once the normal has been calculated, taking the dot product of it with the assumed current sheet normal, perpendicular to the equator, finds the angular offset, revealing the tilt of the current sheet. The results are

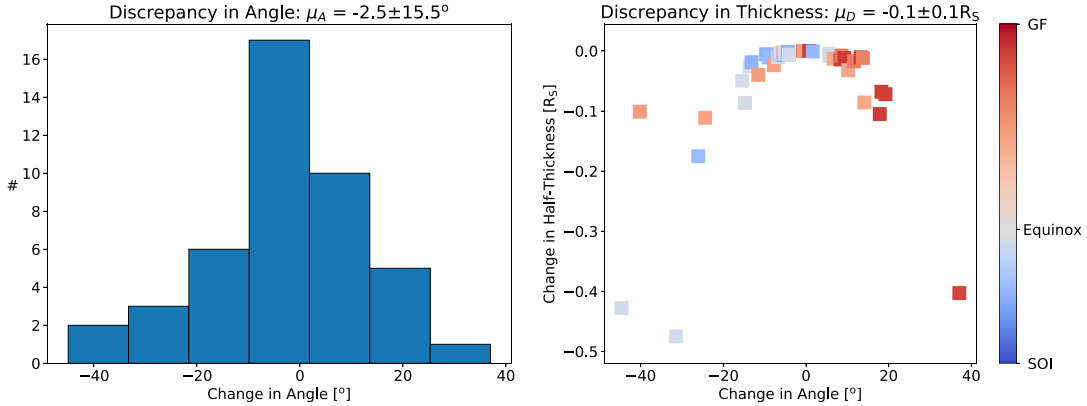

Figure 2. The discrepancy between the assumed current sheet normal, parallel to the dipole axis, and the calculated normal from the magnetic field data, due to the tilt of the current sheet. The left panel shows a histogram of the angular offsets, where the normal was calculated either using Minimum Variance Analysis (MVA) or the Coplanarity Method, depending on which technique had the smallest associated errors. The plot title shows the mean tilt of the current sheet, μ_A, and 1 standard deviation in degrees. In the right panel, the change in thickness is plot with respect to the associated angular discrepancies, where the color represents the time of crossing, ranging between Saturn Orbital Insertion (SOI) in July 2004 and Cassini's end of mission phase, known as the Grand Finale (GF), in September 2017. The color bar changes from blue to red at Saturn's Equinox in August 2009. The plot title shows the mean change in thickness, μ_D, and 1 standard deviation in units of R_S.

shown in the left panel of Figure 2, where a negative offset implies the field is bent southward and a positive offset implies the field is bent northward. We see that the current sheet normal is most often found to be almost aligned with the assumed normal, where the maximum displacement was $\pm 40°$. To see how this reduces the half thickness, we multiply our calculated half-thickness values by $\sin\theta$ where θ is the change in angle. These results are shown in the right panel of Figure 2. The change in angle is mostly well organized by season; however, there is some variability, revealing the dynamic structure of the current sheet. The average decrease in half-thickness is 0.1 R_S with a maximum decrease of 0.5 R_S, but there were only three cases where the decrease was this large, with most of the changes clustered around -0.1 R_S. This implies that there is only a minor change in the thickness if the current sheet normal is not assumed to be perpendicular to the rotational equator. However, we must consider the errors associated with MVA and the Coplanarity Method. For some cases the errors were too large to make the calculated normal trustworthy, most commonly due to the time taken for a crossing. In addition, while we expect this to be one of the most significant sources of error, there are other potential sources that we have not considered. Therefore, we define an approximate order of magnitude error in the calculated half-thickness for all our crossings to be ± 0.1 R_S.

We show two example orbits where we have used the method outlined herein to determine the current sheet thickness in Figure 1. For Rev 114, shown in the left panels of Figure 1, the half-thickness of the current sheet was 1.0 R_S and the offset of the center was 0.1 R_S. This crossing occurred at ~8 R_S on the dayside, around 10 a.m. local time and took approximately ~4 hr to pass through the current sheet. In this case the current sheet was particularly thin and close to the equator. The current sheet is expected to be almost colocated with the rotational equator since it occurred in 2009, close to equinox. For Rev 195, shown in the right panels of Figure 1, the half thickness was 2.2 R_S and the offset was 0.3 R_S. Since this crossing occurred in 2013 during northern summer, the positive offset is unexpected. The orbits that preceded this example were checked and while they occurred at almost identical radial distances and local times, the offset, as well as the thickness, was not the same in each case, showing evidence of temporal variability. For Rev 195, Cassini took approximately ~10 hr to traverse the current sheet, almost the length of a PPO cycle, which could imply that the current sheet has moved while Cassini passes through. We chose not to set an upper limit on the time taken for a crossing because this would limit the maximum thickness that can be directly measured and so we include all examples that fulfilled the criteria we have set out.

Figure 1e shows data from the CAPS Electron Spectrometer (Young et al., 2004), an instrument that measured electron distributions between 0.5 eV and 28 keV, from which the moments can be calculated, as described by Lewis et al. (2008). For Rev 114 the plasma sheet appears to be asymmetric about the current sheet center, where the peak central sheet thermal electron density is $\sim 3\times10^6 m^{-3}$. Whether this asymmetry is temporal or spatial is difficult to determine using in situ data. For instance, the plasma sheet could

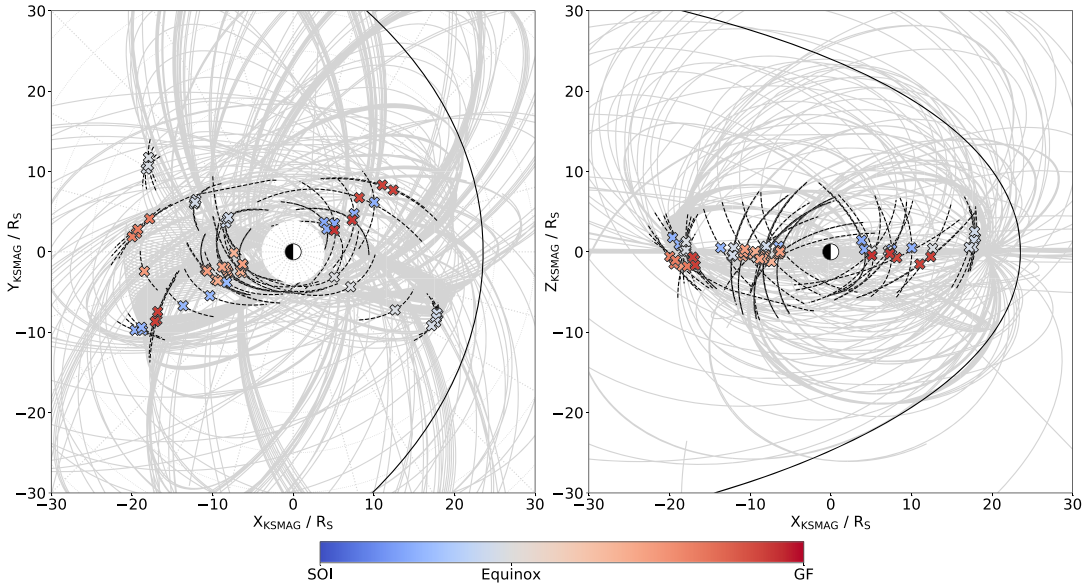

Figure 3. The complete Cassini mission trajectory is shown in light gray with a dawn-dusk asymmetric magnetopause (Pilkington et al., 2015) for a solar wind dynamic pressure of 0.01 nPa shown in black, projected onto the equatorial plane in the left panel and onto the meridional plane in the right panel. The dashed black lines show the trajectory of Cassini 12 hr either side of the current sheet boundaries during each of our 66 events. The crosses show the location of the current sheet center during each crossing and are color coded by time using the same color bar as the previous figure.

be moving southward as Cassini is passing through it. For Rev 195, there was no data collected because the instrument was turned off in 2012, hence why Figure 1j is empty. Sergis et al. (2011) compared the properties of the current and plasma sheets, showing that these two systems can behave independently. In some cases they observed an increase in the current sheet thickness but not the plasma sheet, with the peak plasma sheet density and pressure remaining the same.

The location of each current sheet crossing we have identified are shown in Figure 3. The left panel shows the local time distribution, where the crosses show the location of the current sheet center for each event. The v_z constraint prevents us from using the data at dawn and dusk because Cassini was either moving too slowly, was at the equator when it encountered the current sheet, or Cassini made a fast steep crossing of the equator within the inner edge of the orbit of Enceladus. Therefore, our analysis of the thickness is restricted to the near-noon and near-midnight sectors. The right panel of Figure 3 plots the latitudinal distribution of the crossings, showing that they all occur close to the equator, well within our $\pm 5\,R_S$ boundary and appear to be well separated by season. However, there is some variability in the location of the current sheet center which will be explored. In Figure 3, the dashed black lines show the trajectory of Cassini 12 hr either side of the current sheet boundaries for each crossing. We can clearly see that for each event Cassini made a fast, steep traversal through the equatorial region, allowing for a direct determination of the current sheet properties.

4. Results

We have a catalog of 66 current sheet crossings that have significant spatial and temporal coverage. We find that the median current sheet half thickness is 1.3 R_S, thinner than the initial calculations for the half thickness from early flybys of 2.5 R_S (Bunce & Cowley, 2003; Connerney et al., 1981b; Giampieri & Dougherty, 2004), but within the range of values calculated by Kellett et al. (2009). The interquartile range of this data set is 1 R_S and skewed toward smaller values, implying that the current sheet thickness is highly variable and more often thinner than the median. The thinnest value found was 0.4 R_S and the thickest value was 3.2 R_S, both of which were observed on the nightside, revealing the nightside current sheet to be highly variable. The range of values is greater than that calculated by Kellett et al. (2009), predominantly reflecting our larger data set that covers more of the Saturnian system. For instance, our thinnest value is found at $\rho = 21\,R_S$ on the nightside, a distance outside the presumed outer edge of the current sheet by Kellett et al. (2009). Modeling of the tail current sheet using equatorial data has found even larger half-thickness values $> 10\,R_S$ at greater radial distances (Arridge et al., 2011; Martin & Arridge, 2017). The v_z constraint limits us

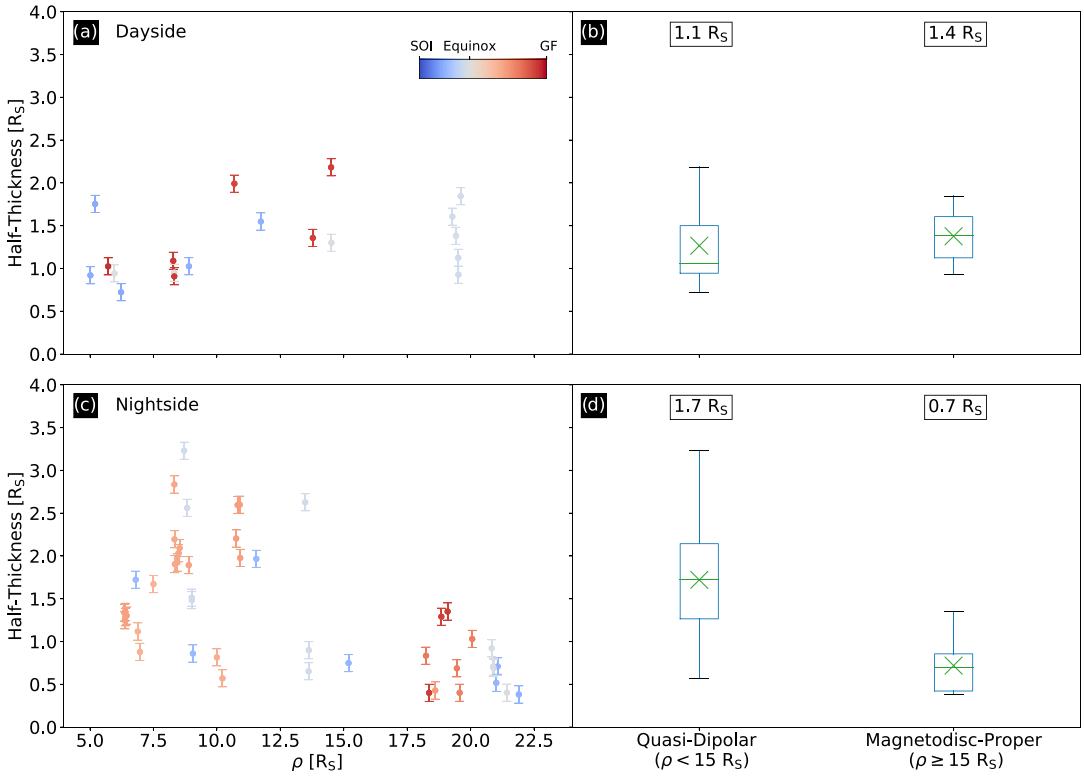

Figure 4. The top two panels show the half-thickness calculated for all dayside magnetodisc current sheet crossing events, while the bottom two panels are for the nightside events. Panels (a) and (c) plots the half thickness as a function of radial distance, color coded by season. Panels (b) and (d) are box plots of the half-thickness binned into the two radial regions, showing the median, interquartile ranges, maximum and minimum values and the mean is also shown by the green cross. The values at the top of panels (b) and (d) show the median current sheet thickness in each region, in units of R_S.

from using data at these radial distances because Cassini was at the slowest point of its orbit. The current sheet would pass through the slowly moving spacecraft and so the change in Cassini's z position between each boundary would be small, giving an underestimate of the thickness. The v_z threshold is predominantly satisfied when ρ is less than 25 R_S and so we focus on data within this radial distance.

4.1. Spatial Variability

To test whether there is a thickness spatial dependency, the data are separated into dayside and nightside local time sectors, and binned into two radial ranges—the quasi-dipolar region ($< 15\,R_S$) and the magnetodisc proper ($\geq 15\,R_S$). This is shown in Figure 4, revealing both a day-night thickness asymmetry, and a radial dependence.

Figures 4a and 4b show the thickness of the 19 dayside events as a function of their perpendicular distance from the spin axis, ρ. The median dayside half thickness is 1.1 R_S, marginally thinner than the global average, but with an interquartile range of 0.6 R_S, revealing some variability about this average value. In panel (b), where the data have been binned into the two radial ranges, the current sheet appears to get slightly thicker with radial distance, from $1.1^{+0.4}_{-0.1}\,R_S$ to $1.4^{+0.2}_{-0.3}R_S$. However, we see that these are within error of each other, where the interquartile ranges of the two box plots overlap. Considering that the magnetodisc proper only contains four data points, it is difficult to claim this is a real radial profile. What we do observe is that the thickness remains within a small range of values on the dayside, implying that the current sheet thickness is not highly variable. On average the current sheet remains approximately constant with radial distance. This could be reflective of the dayside magnetosphere being compressed by the solar wind, preventing the magnetodisc geometry from forming and the current sheet from becoming thinner. When the field becomes more radially distended, the highly stretched field concentrates the plasma toward the equator and thins the current sheet. When the dayside magnetosphere is more expanded, due to either low solar wind dynamic pressure (Arridge et al., 2008) or an increase in the internal plasma pressure (Pilkington et al., 2015), the current sheet would be thinner as the field becomes more radial.

Figures 4c and 4d show the thickness of the nightside current sheet. Panel (a) shows the thickness during all 47 available crossings as a function of ρ, while panel (d) shows the data binned into the two radial ranges. The median nightside half-thickness is 1.3 R_S, slightly thicker than the dayside but with a larger interquartile range of 1.2 R_S, revealing the nightside current sheet thickness to be highly variable. Unlike the dayside, there appears to be a radial trend. In the quasi-dipolar region, the average, or nominal, current sheet half thickness is $1.7^{+0.4}_{-0.5} R_S$ and so the spread of values is not significantly skewed either side of the median. The average nightside current sheet is 50% thicker than the dayside and so, while there is marginal overlap between the interquartile ranges of the dayside and nightside quasi-dipolar data, we shall explore what could physically produce this feature.

The presence of some other observed day-night asymmetries within the Saturnian magnetosphere have been explained by a noon-midnight electric field (see review by Thomsen et al., 2012, and references therein). The associated convection pattern with this electric field in the inner region of the magnetosphere is fixed in local time, such that particles drift radially outward at dawn and radially inward at dusk. These drifts have been measured directly using the CAPS Ion Mass Sepctrometer (IMS) data (Wilson et al., 2013). The drift pattern would result in adiabatic heating of the plasma on the nightside and cooling on the dayside. A day-night asymmetry in the plasma temperatures consistent with this has been observed. The temperature of the water group ions sourced from Enceladus are hotter on the nightside compared to the dayside at radial distances less than 15 R_S (Wilson et al., 2017). The higher nightside temperature would imply a larger centrifugal scale height of the current sheet, and so we would expect a thicker current sheet on the nightside compared to the dayside in the quasi-dipolar region as a result of these particle drifts. Why this convection pattern exists is still not completely understood, but our results appear to provide further support for the presence of a noon-midnight electric field at Saturn.

Simulations of the Saturnian magnetosphere by Jia and Kivelson (2016) found a local time asymmetry in the magnetodisc. They identified a thicker current sheet in the middle magnetosphere (9–15 R_S) at dusk compared to dawn, due to the dipolarization of the field as a response to its confinement by the magnetopause, which is closer to the planet at dusk compared to dawn (Pilkington et al., 2015). They found that the plasma does not return to the equator as the flux tubes corotate through the afternoon sector and so this feature could continue through to the nightside, resulting in a thicker current sheet close to the planet. However, on the nightside the field is no longer confined and is able to stretch down tail. Figure 4 shows that the current sheet thins with radial distance on the nightside, revealing the field curvature to be much higher. The sheet reduces in thickness with radial distance by more than a half from an average half-thickness of $1.7^{+0.4}_{-0.5} R_S$ to $0.7^{+0.2}_{-0.3} R_S$, with far less variability in the outer region and no overlap between the errors associated with each radial range. This suggests that this is a real radial profile of the current sheet thickness on the nightside.

This observed day-night asymmetry in current sheet thickness could also be reflective of the inherent difference in field geometry at similar radial distances on the nightside and dayside. If we consider the distance between the equator and magnetopause at a given radial distance, it will be larger on the nightside than the dayside due to the polar flattening of the magnetopause. In the right panel of Figure 3, at $x = 10\,R_S$ on the dayside, the magnetopause boundary is at approximately $z = 20\,R_S$. But on the nightside at $x = -10\,R_S$ the boundary is at $z = 30\,R_S$. The magnetic field is less confined, which could allow the plasma to expand further along the field lines, increasing the current sheet thickness.

4.2. Temporal Variability

A difficulty using in situ measurements is separating spatial and temporal variability. We must consider whether the spatial day-night asymmetry is a result of a temporal observation bias. The PPOs are ubiquitous within the Saturnian magnetosphere and so we consider the effect these might have on our data set. When the PPO systems are in phase, the thickness modulations are expected to be smaller compared to when they are in antiphase. If the dayside was measured more frequently during in-phase conditions compared to the nightside, this could explain the observed asymmetry. To test this, during each crossing we look at $\Phi_{N,S}$, the global phases of the PPOs that have been determined for the complete Cassini mission (Andrews et al., 2008, 2012; Cowley & Provan, 2015, 2016; Gurnett et al., 2009, 2011; Kurth et al., 2007;2008; Lamy, 2011, 2017; Provan et al., 2013, 2014, 2016, 2019). We first transform the global phases $\Phi_{N,S}$ into a local phases, to account for both Cassini's position in local time and a $3^\circ R_S^{-1}$ radial phase delay that is expected when Cassini is outside of the core PPO region, at distances $\rho > 12\,R_S$ (Arridge et al., 2011; Provan et al., 2012). These new phase values are given by $\Psi^*_{N,S}$. The relative phase of the PPOs, or beat phase, is therefore given

by $\Delta\Psi^* = \Psi^*_N - \Psi^*_S$. The variation in beat phase during a single crossing is small and so we use the beat phase calculated at the current sheet center for each crossing. The events within the dayside and nightside quasi-dipolar region are separated by their beat phase. When $\Delta\Psi^* = 0 \pm 90°$, we say that the PPOs are in-phase, and when $\Delta\Psi^* \approx 180 \pm 90°$ they are in antiphase. Each bin will therefore contain crossings that occurred when the PPO current systems were in quadrature ($\Delta\Psi^* \approx 90°$ and $\Delta\Psi^* \approx 270°$). Nonetheless, even with this wider range we would still expect to see the largest thickness modulations to occur during antiphase conditions.

We find that both the nightside and dayside current sheet are slightly thicker than the average value shown in Figure 2 in the quasi-dipolar region during antiphase conditions. The median dayside current sheet half thickness is $1.4^{+0.5}_{-0.2}\,R_S$ and the nightside is $1.9 \pm 0.5\,R_S$, showing a increase of 30% and 10%, respectively, although we note that there is some overlap between their associated errors. Hence we see a greater difference for the dayside, yet still observe on average a thinner current sheet compared to the nightside. During in-phase conditions, the average dayside half thickness decreases to 1.1 R_S, with negligible error bars due to only having a few data points, and the average nightside half-thickness decreases to $1.4^{+0.5}_{-0.2}\,R_S$, both reducing on average by 20%. While there appears to be a beat phase thickness dependence, they have a similar effect for both local time sectors. This suggests that the day-night thickness asymmetry is not due to a PPO beat phase observation bias.

To determine whether there is a thickness seasonal dependence, Figure 4 also shows the time of Saturn's year for each crossing. The results do not appear to have any clear ordering with respect to time. If the current sheet was thinnest close to equinox, we would expect to see the light blue and red points below the darker blue and red points. However, while we observe variability in the thickness shown in Figure 4, there is no clear preference for a thicker or thinner current sheet during a specific period of Saturn's year. Our results do not provide any clear evidence for a thickness seasonal dependence.

While we have considered how well the thickness modulations are ordered by the beat phase of the PPOs, we now consider the northern and southern PPO phases during each crossing. We separate the data into each local time and radial bin during both in-phase and antiphase conditions to look for a PPO dependence. When $\Psi^*_S = 0°$ and $\Psi^*_N = 180°$, the meridional component of the perturbation magnetic field produced by the PPOs adds to the southward directed background field and subtracts from it when $\Psi^*_S = 180°$ and $\Psi^*_N = 0°$. We therefore expect the current sheet to be thicker when $\Psi^*_S = 0°$ and $\Psi^*_N = 180°$, since the equatorial field strength has increased, and thinner in the opposite case (see Figure 2 in Cowley & Provan, 2017). When the two current systems are in phase, we would expect the thickness modulations due to each current system to approximately cancel, whereas when the systems are in antiphase, we would expect the thickness modulations to add.

We begin by looking at the PPO phases during each crossing. Since the time taken for Cassini to traverse the current sheet varies between 3–18 hr for our set of events, the northern and southern phases will vary during a crossing. Hence, for each event we calculate the directional mean and circular standard deviation (Mardia & Jupp, 2000) of $\Psi^*_{N,S}$. This tells us the average phase during a crossing and the standard deviation represents the range of phases during a crossing. If the standard deviation is large, Cassini spent a significant period of time within the current sheet. We remove the 12 events that took longer than an approximate PPO cycle (~11 hr) from this part of the analysis, leaving us with 54 events.

Figures 5a and 5b plots the thickness and offset, respectively, as a function of Ψ^*_S, for crossings that occurred in the nightside magnetodisc proper region. There are 14 events that occurred between 2007 and 2016. Figures 5c and 5d show data from the quasi-dipolar region. There are 25 events that occurred between 2007 and 2013. A sine curve was fit to the data to determine whether the variability in thickness is well described by the expected PPO modulations from both the northern and southern phases. The amplitude, phase offset, and central value were free parameters, which reveal the magnitude of the PPO modulation, phase delay, and the unperturbed half-thickness, respectively. The horizontal error bars show the circular standard deviation. The vertical error bars show the error associated with determining the thickness. A $\pm 0.1\,R_S$ error is applied to the measured current sheet offset.

Figure 5a shows that the thickness modulations in the nightside magnetodisc proper appear to be reasonably organized by the southern PPO phase. The fitting procedure found a nominal current sheet half-thickness of 0.7 R_S, the same as the value found in Figure 4. The current sheet half thickness varies between 0.4 R_S

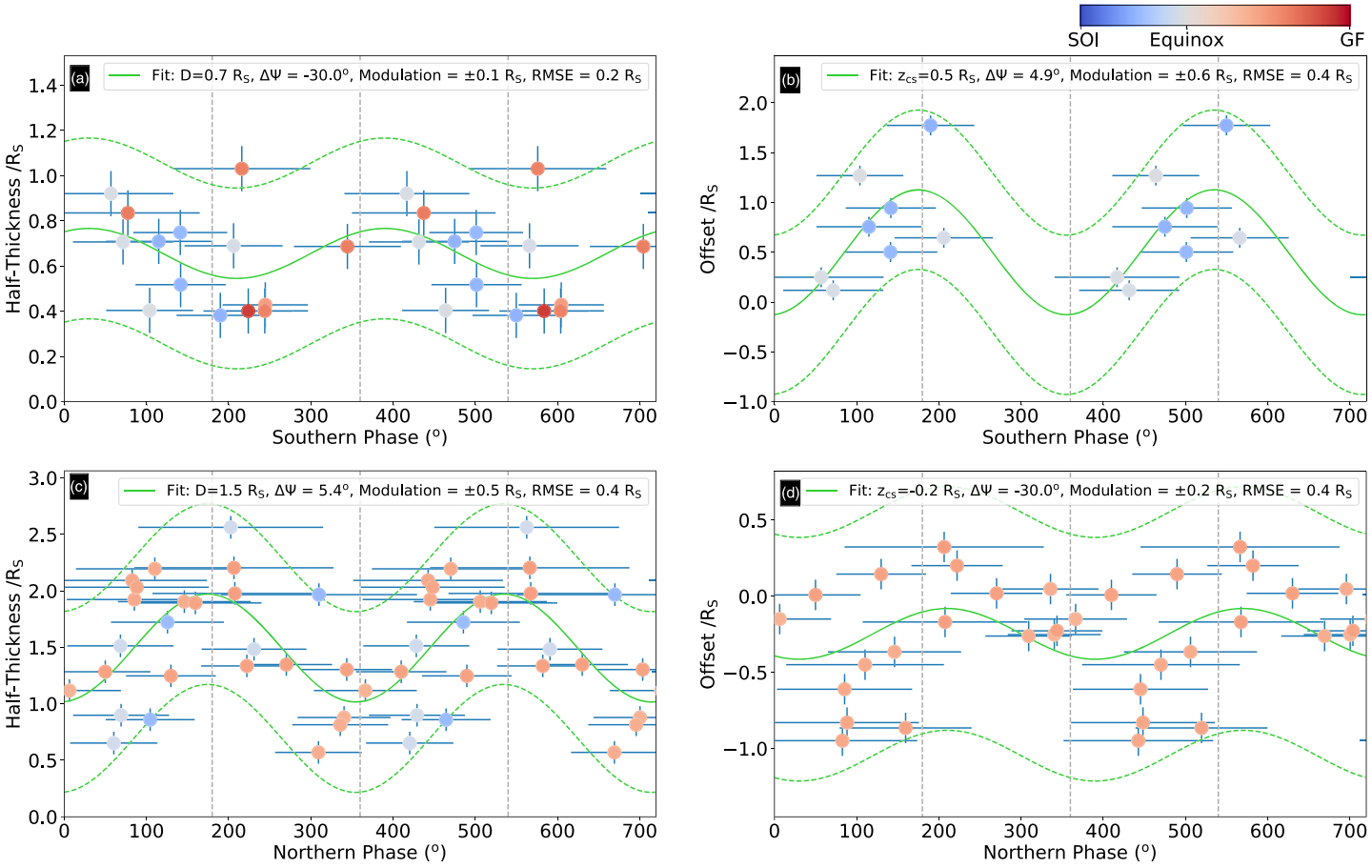

Figure 5. Panels (a) and (c) show the half thickness, given by D, for crossings on the nightside in the magnetodisc proper and quasi-dipolar regions as a function of the local southern PPO phase and northern PPO phase, respectively. A fitted sine curve is plot on top, revealing the magnitude of the modulation and the nominal thickness. Panels (b) and (d) show the calculated offset, given by z_{CS}, and a fitted sinusoid for a subset of the data in (a) and (c), restricted to events that occurred either preequinox or postequinox. The phase delay, given by ΔΨ, modulation amplitude, and root-mean-square error (RMSE) of the fit are shown in the legend of each plot. The 95% confidence interval is also shown (as dashed lines) for each fitted sinusoid.

and 1.0 R_S and appears to follow a sinusoidal variation quite well, with a root-mean-square error (RMSE) of 0.2 R_S, assuming a modulation of $\pm 0.1\,R_S$. However, not all the data follow this trend, with an example of a thick current sheet at $\Psi_S^* = 180°$ when it is expected to be thinner than on average. However, if all the thickness modulations were be mapped by a simple sinusoidal variation, this would assume the only source of variability are the PPOs. While Figure 5a appears to show that the PPOs could be one of the main drivers, there seems to be evidence for other sources of thickness variability.

Figure 5b shows a subset of the data from Figure 5a to analyze the behavior of the current sheet offset. The data from Figure 5a contains more events that occurred before 2009, when the current sheet center is expected to be positive since it is southern summer, and so we analyze these events. A sine curve was fit to this subset of examples and revealed a central offset value of 0.5 R_S. Using the Arridge et al. (2008) model, this would imply a hinging distance of 28 R_S, which is within the 16–32 R_S range previously observed (Arridge et al., 2011; Carbary et al., 2015). However, an assumption here is that the current sheet offset is fixed and any variability is due to the PPOs. The hinging distance has been shown to vary orbit-to-orbit due to variable solar wind forcing (Agiwal et al., 2020), and since our events range over 2 years this assumption might not be valid, so it is difficult to separate these two effects.

The data were shown as a function of the southern PPO phase because the RMSE associated with the fits was smaller compared to the northern PPO phase. This could be reflective of the current sheet being more responsive to the southern PPO current system. Determining the relative strength of the PPO current systems reveals which is dominant. The parameter k is the ratio of the amplitude of the northern PPO system

over the southern PPO system and has been calculated for the complete Cassini mission where possible (Andrews et al., 2012; Provan et al., 2013, 2016, 2018). If $k > 1$ the northern system dominates and if $k < 1$ the southern system dominates. The events in Figure 5a occurred during 2007, 2009, 2013, and 2014. During 2007, $k < 1$ so the southern phase dominated, while $k \approx 1$ during the second half of 2009 and the first half of 2013. For the rest of the data there is currently no known k value. All the data in Figure 5b occurred before equinox when $k < 1$ and the southern system dominated so it makes sense for the data to be better organized by the southern PPO phase.

Figure 5c shows the thickness of the magnetodisc current sheet in the nightside quasi-dipolar region ($< 15\,R_S$) as a function of the northern PPO phase. The variations in thickness appear to be somewhat organized by an assumed sinusoidal modulation, with an RMSE of 0.4 R_S. The fit determined a nominal half-thickness of 1.5 R_S, in close agreement with the median calculated using all the data in this region, but slightly thinner, most likely due to our removal of crossings that took longer than a PPO cycle. The half-thickness of the current sheet varies between 0.5–2.5 R_S, showing larger variability than in the magnetodisc proper region. Figure 5d shows a subset of the data that occurred postequinox, when the current sheet offset is expected to be negative. The nominal offset was found to be $-0.2\,R_S$, implying that the hinging distance was 19 R_S, again within the range of previously recorded hinging distances. The events in Figure 5c occurred during 2007, 2009, 2012, and 2013, where $k \lesssim 1$ except for in 2012 when $k > 1$. All the events in Figure 5d occurred postequinox, when $k \geq 1$ and so this would suggest the data should be better organized by the northern PPO phase. However, the difference in RMSE between southern and northern phase organization of the offset was smaller compared to the cases in Figure 5b. This could be because the dominance of the northern PPO system was weaker in 2012 compared to the dominance of the southern PPO system preequinox.

On the dayside, there was minimal thickness and offset variability, as previously discussed, and some of this was quite well organized as a sinusoidal variation. However, the evidence for PPO control was less clear, with more examples that do not follow the trend, where the current sheet was particularly thick or offset. This could be due to variable upstream solar wind conditions resulting in larger displacements and a thicker current sheet. Future work will consider case studies to constrain the thickness variability on the dayside with respect to the properties of the solar wind.

We were unable to identify clear evidence of the expected thickness and offset modulation differences when the PPOs were in phase or in antiphase conditions that has previously been discussed (Cowley & Provan, 2017; Provan et al., 2012; Thomsen et al., 2017). For instance, on the nightside in the magnetodisc proper region during antiphase conditions, we see a sinusoidal variation in the current sheet thickness. However, during in-phase conditions, while the range of measured thickness values reduced by 50%, as we would expect, the variability is not well mapped by the simple sinusoidal relation. It should be noted that the set of crossings occur throughout the complete Cassini mission and so k is variable between events. This changes the expected modulation of the thickness and offset by the PPOs. In addition, the $\pm 90°$ range for the in-phase and anti-phase conditions introduces cases when the PPO systems were in quadrature. This could make identifying the differences between these two conditions less clear.

5. Conclusion

We have determined the nominal thickness of the magnetodisc current sheet and analyzed potential sources of variability. Using a simple variance analysis, the thickness was uniquely determined when Cassini made fast, steep crossings of the current sheet. The average half-thickness of the current sheet is 1.3 R_S; however, evidence for both spatial and temporal variability was found. On the dayside, the current sheet has an approximately constant thickness with respect to radial distance from the planet, most likely reflecting the compression of the dayside magnetosphere by the solar wind. On the nightside, the current sheet is thicker than the dayside close to the planet. These results are consistent with and support the presence of a noon-midnight electric field at Saturn that produces a hotter plasma population on the nightside compared to the dayside, resulting in a thicker current sheet. The current sheet was further shown to get significantly thinner with radial distance on the nightside as the magnetic field stretches down into the tail. Some of the variability in thickness was shown to be somewhat characterized by the PPOs. However, there also appears to be evidence for other sources of variability.

These results reveal how the current sheet responds to processes that drive large-scale dynamics at Saturn. The thickness values calculated are essential for accurately modeling the current sheet and show the requirement for considering both the spatial and temporal variability of the largest current system in the Saturnian magnetosphere.

Acknowledgments
N. R. S. is funded by the STFC DTP Studentship. M. K. D. is supported by a Royal Society Research Professorship. A. M. is supported by a Royal Society University Research Fellowship. E. J. B. is supported by an STFC Consolidated Grant and the Royal Society Wolfson Research Merit Award. The calibrated 1 min resolution Cassini magnetic field data in KSM coordinates are available at the Planetary Plasma Interaction (PPI) Node of NASA's Planetary Data System (PDS) (https://pds-ppi.igpp.ucla.edu/) in the folder CO-E/SW/J/S-MAG-4-SUMM-1MINAVG-V2.0. The Cassini Plasma Spectrometer (CAPS) Derived Electron Moments from the Electron Spectrometer (ELS) is available at the PPI Node of the PDS in the folder CO-E/J/S/SW-CAPS-5-DDR-ELE-MOMENTS-V1.0. We would like to thank Gabrielle Provan for providing the phases of the PPOs.

References

Agiwal, O., Hunt, G. J., Dougherty, M. K., Cowley, S. W. H., & Provan, G. (2020). Modeling the temporal variability in Saturn's magnetotail current sheet from the Cassini F-ring orbits. *Journal of Geophysical Research: Space Physics*, *125*, e2019JA027371. https://doi.org/10.1029/2019JA027371

Andrews, D. J., Bunce, E. J., Cowley, S. W. H., Dougherty, M. K., Provan, G., & Southwood, D. J. (2008). Planetary period oscillations in Saturn's magnetosphere: Phase relation of equatorial magnetic field oscillations and Saturn kilometric radiation modulation. *Journal of Geophysical Research: Space Physics*, *113*, A09205. https://doi.org/10.1029/2007JA012937

Andrews, D. J., Cowley, S. W. H., Dougherty, M. K., Lamy, L., Provan, G., & Southwood, D. J. (2012). Planetary period oscillations in Saturn's magnetosphere: Evolution of magnetic oscillation properties from southern summer to post-equinox. *Journal of Geophysical Research*, *117*, A04224. https://doi.org/10.1029/2011JA017444

Arridge, C. S., André, N., Khurana, K. K., Russell, C. T., Cowley, S. W. H., Provan, G., et al. (2011). Periodic motion of Saturn's nightside plasma sheet. *Journal of Geophysical Research*, *116*, A11205. https://doi.org/10.1029/2011JA016827

Arridge, C. S., Khurana, K. K., Russell, C. T., Southwood, D. J., Achilleos, N., Dougherty, M. K., et al. (2008). Warping of Saturn's magnetospheric and magnetotail current sheets. *Journal of Geophysical Research*, *113*, A08217. https://doi.org/10.1029/2007JA012963

Arridge, C. S., Russell, C. T., Khurana, K. K., Achilleos, N., Cowley, S. W. H., Dougherty, M. K., et al. (2008). Saturn's magnetodisc current sheet. *Journal of Geophysical Research*, *113*, A04214. https://doi.org/10.1029/2007JA012540

Bagenal, F., & Delamere, P. A. (2011). Flow of mass and energy in the magnetospheres of Jupiter and Saturn. *Journal of Geophysical Research*, *116*, A05209. https://doi.org/10.1029/2010JA016294

Bradley, T. J., Cowley, S. W. H., Bunce, E. J., Smith, A. W., Jackman, C. M., & Provan, G. (2018). Planetary period modulation of reconnection bursts in Saturn's magnetotail. *Journal of Geophysical Research: Space Physics*, *123*, 9476–9507. https://doi.org/10.1029/2018JA025932

Bunce, E. J., Arridge, C. S., Cowley, S. W. H., & Dougherty, M. K. (2008). Magnetic field structure of Saturn's dayside magnetosphere and its mapping to the ionosphere: Results from ring current modeling. *Journal of Geophysical Research*, *113*, A02207. https://doi.org/10.1029/2007JA012538

Bunce, E. J., & Cowley, S. W. H. (2003). A note on the ring current in Saturn's magnetosphere: Comparison of magnetic data obtained during the Pioneer-11 and Voyager-1 and -2 fly-bys. *Annales Geophysicae*, *21*(3), 661–669. Retrieved from https://hal.archives-ouvertes.fr/hal-00317009

Bunce, E. J., Cowley, S. W. H., Alexeev, I. I., Arridge, C. S., Dougherty, M. K., Nichols, J. D., & Russell, C. T. (2007). Cassini observations of the variation of Saturn's ring current parameters with system size. *Journal of Geophysical Research*, *112*, A10202. https://doi.org/10.1029/2007JA012275

Carbary, J. F., & Mitchell, D. G. (2013). Periodicities in Saturn's magnetosphere. *Reviews of Geophysics*, *51*(1), 1–30. https://doi.org/10.1002/rog.20006

Carbary, J. F., Sergis, N., Mitchell, D. G., & Krupp, N. (2015). Saturn's hinge parameter from Cassini magnetotail passes in 2013–2014. *Journal of Geophysical Research: Space Physics*, *120*, 4438–4445. https://doi.org/10.1002/2015JA021152

Connerney, J. E. P., Acuna, M. H., & Ness, N. F. (1981a). Modeling the Jovian current sheet and inner magnetosphere. *Journal of Geophysical Research*, *86*, 8370–8384. https://doi.org/10.1029/JA086iA10p08370

Connerney, J. E. P., Acuna, M. H., & Ness, N. F. (1981b). Saturn's ring current and inner magnetosphere. *Nature*, *292*, 724–726. https://doi.org/10.1038/292724a0

Cowley, S. W. H., Nichols, J. D., & Jackman, C. M. (2015). Down-tail mass loss by plasmoids in Jupiter's and Saturn's magnetospheres. *Journal of Geophysical Research: Space Physics*, *120*, 6347–6356. https://doi.org/10.1002/2015JA021500

Cowley, S. W. H., & Provan, G. (2015). Planetary period oscillations in Saturn's magnetosphere: Comments on the relation between post-equinox periods determined from magnetic field and skr emission data. *Annales Geophysicae*, *33*(7), 901–912. Retrieved for https://www.ann-geophys.net/33/901/2015/

Cowley, S. W. H., & Provan, G. (2016). Planetary period oscillations in Saturn's magnetosphere: Further comments on the relationship between post-equinox properties deduced from magnetic field and Saturn kilometric radiation measurements. *Icarus*, *272*, 258–276. https://doi.org/10.1016/j.icarus.2016.02.051

Cowley, S. W. H., & Provan, G. (2017). Planetary period modulations of Saturn's magnetotail current sheet during northern spring: Observations and modeling. *Journal of Geophysical Research: Space Physics*, *122*, 6049–6077. https://doi.org/10.1002/2017JA023993

Cowley, S. W. H., Provan, G., Hunt, G. J., & Jackman, C. M. (2017). Planetary period modulations of Saturn's magnetotail current sheet: A simple illustrative mathematical model. *Journal of Geophysical Research: Space Physics*, *122*, 258–279. https://doi.org/10.1002/2016JA023367

Dougherty, M. K., Cao, H., Khurana, K. K., Hunt, G. J., Provan, G., Kellock, S., et al. (2018). Saturn's magnetic field revealed by the Cassini grand finale. *Science*, *362*, eaat5434. https://doi.org/10.1126/science.aav6732

Dougherty, M. K., Kellock, S., Southwood, D. J., Balogh, A., Smith, E. J., Tsurutani, B. T., et al. (2004). The Cassini magnetic field investigation. *Space Science Reviews*, *114*, 331–383. https://doi.org/10.1007/s11214-004-1432-2

Dougherty, M. K., Khurana, K. K., Neubauer, F. M., Russell, C. T., Saur, J., Leisner, J. S., & Burton, M. E. (2006). Identification of a dynamic atmosphere at Enceladus with the Cassini magnetometer. *Science*, *311*(5766), 1406–1409. https://doi.org/10.1126/science.1120985

Dungey, J. W. (1961). Interplanetary magnetic field and the auroral zones. *Physical Review Letters*, *6*, 47–48. https://doi.org/10.1103/PhysRevLett.6.47

Edwards, T. M., Bunce, E. J., & Cowley, S. W. H. (2001). A note on the vector potential of Connerney et al.'s model of the equatorial current sheet in Jupiter's magnetosphere. *Planetary and Space Science*, *49*, 1115–1123. https://doi.org/10.1016/S0032-06330000164-1

Giampieri, G., & Dougherty, M. (2004). Modelling of the ring current in Saturn's magnetosphere. *Annales Geophysicae*, *22*, 653–659. https://doi.org/10.5194/angeo-22-653-2004

Gurnett, D. A., Groene, J. B., Averkamp, T. F., Kurth, W. S., Ye, S. Y., & Fischer, G. (2011). An SLS4 longitude system based on a tracking filter analysis of the rotational modulation of Saturn kilometric radiation. In H. O. Rucker, W. S. Kurth, P. Louarn, & G. Fischer (Eds.), *Planetary, solar and heliospheric radio emissions (pre vii)* (pp. 51–64). Vienna, Austria: Austrian Academy of Sciences.

Gurnett, D. A., Lecacheux, A., Kurth, W. S., Persoon, A. M., Groene, J. B., Lamy, L., et al. (2009). Discovery of a north-south asymmetry in Saturn's radio rotation period. *Geophysical Research Letters*, *36*, L16102. https://doi.org/10.1029/2009GL039621

Harris, E. G. (1962). On a plasma sheath separating regions of oppositely directed magnetic field. *Il Nuovo Cimento (1955-1965)*, *23*(1), 115–121. https://doi.org/10.1007/BF02733547

Hill, T. W., & Michel, F. C. (1976). Heavy ions from the Galilean satellites and the centrifuga distortion of the Jovian magnetosphere. *Journal of Geophysical Research*, *81*(25), 4561–4565. https://doi.org/10.1029/JA081i025p04561

Hunt, G. J., Cowley, S. W. H., Provan, G., Bunce, E. J., Alexeev, I. I., Belenkaya, E. S., et al. (2014). Field-aligned currents in Saturn's southern nightside magnetosphere: Subcorotation and planetary period oscillation components. *Journal of Geophysical Research: Space Physics*, *119*, 9847–9899. https://doi.org/10.1002/2014JA020506

Hunt, G. J., Cowley, S. W. H., Provan, G., Bunce, E. J., Alexeev, I. I., Belenkaya, E. S., et al. (2015). Field-aligned currents in Saturn's northern nightside magnetosphere: Evidence for interhemispheric current flow associated with planetary period oscillations. *Journal of Geophysical Research: Space Physics*, *120*, 7552–7584. https://doi.org/10.1002/2015JA021454

Hunt, G. J., Cowley, S. W. H., Provan, G., Bunce, E. J., Alexeev, I. I., Belenkaya, E. S., et al. (2016). Field-aligned currents in Saturn's magnetosphere: Local time dependence of southern summer currents in the dawn sector between midnight and noon. *Journal of Geophysical Research: Space Physics*, *121*, 7785–7804. https://doi.org/10.1002/2016JA022712

Jackman, C. M., & Arridge, C. S. (2011). Statistical properties of the magnetic field in the Kronian magnetotail lobes and current sheet. *Journal of Geophysical Research*, *116*, A05224. https://doi.org/10.1029/2010JA015973

Jackman, C. M., Thomsen, M. F., & Dougherty, M. K. (2019). Survey of Saturn's magnetopause and bow shock positions over the entire Cassini mission: Boundary statistical properties and exploration of associated upstream conditions. *Journal of Geophysical Research: Space Physics*, *124*, 8865–8883. https://doi.org/10.1029/2019JA026628

Jia, X., & Kivelson, M. G. (2016). Dawn-dusk asymmetries in rotating magnetospheres: Lessons from modeling Saturn. *Journal of Geophysical Research: Space Physics*, *121*, 1413–1424. https://doi.org/10.1002/2015JA021950

Jia, X., Kivelson, M. G., & Gombosi, T. I. (2012). Driving Saturn's magnetospheric periodicities from the upper atmosphere/ionosphere. *Journal of Geophysical Research*, *117*, A04215. https://doi.org/10.1029/2011JA017367

Kawano, H., & Higuchi, T. (1995). The bootstrap method in space physics: Error estimation for the minimum variance analysis. *Geophysical Research Letters*, *22*(3), 307–310. https://doi.org/10.1029/94GL02969

Kellett, S., Bunce, E. J., Coates, A. J., & Cowley, S. W. H. (2009). Thickness of Saturn's ring current determined from north-south Cassini passes through the current layer. *Journal of Geophysical Research: Space Physics*, *114*, A04209. https://doi.org/10.1029/2008JA013942

Kurth, W. S., Averkamp, T. F., Gurnett, D. A., Groene, J. B., & Lecacheux, A. (2008). An update to a saturnian longitude system based on kilometric radio emissions. *Journal of Geophysical Research*, *113*, A05222. https://doi.org/10.1029/2007JA012861

Kurth, W. S., Lecacheux, A., Averkamp, T. F., Groene, J. B., & Gurnett, D. A. (2007). A saturnian longitude system based on a variable kilometric radiation period. *Geophysical Research Letters*, *34*, L02201. https://doi.org/10.1029/2006GL028336

Lamy, L. (2011). Variability of southern and northern periodicities of Saturn kilometric radiation. In H. O. Rucker, W. S. Kurth, P. Louarn, & G. Fischer (Eds.), *Planetary, solar and heliospheric radio emissions (PRE VII)* (pp. 39–50). Vienna, Austria: Austrian Academy of Sciences.

Lamy, L. (2017). The Saturnian kilometric radiation before the Cassini Grand Finale, *Planetary radio emissions viii* (pp. 171–190). Vienna, Austria: Austrian Academy of Sciences. https://doi.org/10.1553/PRE8s171

Lewis, G. R., André, N., Arridge, C. S., Coates, A. J., Gilbert, L. K., Linder, D. R., & Rymer, A. M. (2008). Derivation of density and temperature from the Cassini-Huygens caps electron spectrometer. *Planetary and Space Science*, *56*(7), 901–912. https://doi.org/10.1016/j.pss.2007.12.017

Mardia, K. V., & Jupp, P. E. (2000). Directional statistics. Chichester, UK: J. Wiley and Sons Ltd.

Martin, C., & Arridge, C. S. (2017). Cassini observations of aperiodic waves on Saturn's magnetodisc. *Journal of Geophysical Research: Space Physics*, *122*, 8063–8077. https://doi.org/10.1002/2017JA024293

Pilkington, N. M., Achilleos, N., Arridge, C. S., Guio, P., Masters, A., Ray, L. C., & Sergis, N. (2015). Internally driven large-scale changes in the size of Saturn's magnetosphere. *Journal of Geophysical Research*, *120*, 7289–7306. https://doi.org/10.1002/2015JA021290

Pilkington, N. M., Achilleos, N., Arridge, C. S., Guio, P., Masters, A., Ray, L. C., et al. (2015). Asymmetries observed in Saturn's magnetopause geometry. *Geophysical Research Letters*, *42*, 6890–6898. https://doi.org/10.1002/2015GL065477

Provan, G., Andrews, D. J., Arridge, C. S., Coates, A. J., Cowley, S. W. H., Cox, G., et al. (2012). Dual periodicities in planetary-period magnetic field oscillations in Saturn's tail. *Journal of Geophysical Research*, *117*, A01209. https://doi.org/10.1029/2011JA017104

Provan, G., Cowley, S. W. H., Bradley, T. J., Bunce, E. J., Hunt, G. J., & Dougherty, M. K. (2018). Planetary period oscillations in Saturn's magnetosphere: Cassini magnetic field observations over the northern summer solstice interval. *Journal of Geophysical Research: Space Physics*, *123*, 3859–3899. https://doi.org/10.1029/2018JA025237

Provan, G., Cowley, S. W. H., Lamy, L., Bunce, E. J., Hunt, G. J., Zarka, P., & Dougherty, M. K. (2016). Planetary period oscillations in Saturn's magnetosphere: Coalescence and reversal of northern and southern periods in late northern spring. *Journal of Geophysical Research: Space Physics*, *121*, 9829–9862. https://doi.org/10.1002/2016JA023056

Provan, G., Cowley, S. W. H., Sandhu, J., Andrews, D. J., & Dougherty, M. K. (2013). Planetary period magnetic field oscillations in Saturn's magnetosphere: Postequinox abrupt nonmonotonic transitions to northern system dominance. *Journal of Geophysical Research: Space Physics*, *118*, 3243–3264. https://doi.org/10.1002/jgra.50186

Provan, G., Lamy, L., Cowley, S. W. H., & Bunce, E. J. (2019). Planetary period oscillations in Saturn's magnetosphere: Comparison of magnetic and skr modulation periods and phases during northern summer to the end of the Cassini mission. *Journal of Geophysical Research: Space Physics*, *124*, 1157–1172. https://doi.org/10.1029/2018JA026079

Provan, G., Lamy, L., Cowley, S. W. H., & Dougherty, M. K. (2014). Planetary period oscillations in Saturn's magnetosphere: Comparison of magnetic oscillations and SKR modulations in the postequinox interval. *Journal of Geophysical Research: Space Physics*, *119*, 7380–7401. https://doi.org/10.1002/2014JA020011

Sergis, N., Arridge, C. S., Krimigis, S. M., Mitchell, D. G., Rymer, A. M., Hamilton, D. C., et al. (2011). Dynamics and seasonal variations in Saturn's magnetospheric plasma sheet, as measured by Cassini. *Journal of Geophysical Research*, *116*, A04203. https://doi.org/10.1029/2010JA016180

Smith, C. G. A. (2006). Periodic modulation of gas giant magnetospheres by the neutral upper atmosphere. *Annales Geophysicae*, *24*(10), 2709–2717. https://doi.org/10.5194/angeo-24-2709-2006

Smith, E. J., Davis, L., Jones, D. E., Coleman, P. J., Colburn, D. S., Dyal, P., & Sonett, C. P. (1980). Saturn's magnetosphere and its interaction with the solar wind. *Journal of Geophysical Research*, *85*(A11), 5655–5674. https://doi.org/10.1029/JA085iA11p05655

Smith, H. T., Johnson, R. E., Perry, M. E., Mitchell, D. G., McNutt, R. L., & Young, D. T. (2010). Enceladus plume variability and the neutral gas densities in Saturn's magnetosphere. *Journal of Geophysical Research*, *115*, A10252. https://doi.org/10.1029/2009JA015184

Sonnerup, B. U. Ö., & Scheible, M. (1998). Minimum and maximum variance analysis (Vol. 1).

Sorba, A. M., Achilleos, N. A., Sergis, N., Guio, P., Arridge, C. S., & Dougherty, M. K. (2019). Local time variation in the large-scale structure of Saturn's magnetosphere. *Journal of Geophysical Research: Space Physics*, *124*, 7425–7441. https://doi.org/10.1029/2018JA026363

Southwood, D. J., & Cowley, S. W. H. (2014). The origin of Saturn's magnetic periodicities: Northern and southern current systems. *Journal of Geophysical Research: Space Physics*, *119*, 1563–1571. https://doi.org/10.1002/2013JA019632

Southwood, D. J., & Kivelson, M. G. (2007). Saturnian magnetospheric dynamics: Elucidation of a camshaft model. *Journal of Geophysical Research*, *112*, JA012254. https://doi.org/10.1029/2007JA012254

Staniland, N. R., Dougherty, M. K., & Masters, A. (2018). Quantifying the stress of the Saturnian magnetosphere during the Cassini era. *Geophysical Research Letters*, *45*, 8704–8711. https://doi.org/10.1029/2018GL078815

Thomsen, M. F., Jackman, C. M., Cowley, S. W. H., Jia, X., Kivelson, M. G., & Provan, G. (2017). Evidence for periodic variations in the thickness of Saturn's nightside plasma sheet. *Journal of Geophysical Research: Space Physics*, *122*, 280–292. https://doi.org/10.1002/2016JA023368

Thomsen, M. F., Jackman, C. M., Mitchell, D. G., Hospodarsky, G., Kurth, W. S., & Hansen, K. C. (2015). Sustained lobe reconnection in Saturn's magnetotail. *Journal of Geophysical Research: Space Physics*, *120*, 10,257–10,274. https://doi.org/10.1002/2015JA021768

Thomsen, M. F., Roussos, E., Andriopoulou, M., Kollmann, P., Arridge, C. S., Paranicas, C. P., et al. (2012). Saturn's inner magnetospheric convection pattern: Further evidence. *Journal of Geophysical Research*, *117*, A09208. https://doi.org/10.1029/201JA017482

Vasyliunas, V. M. (1983). Plasma distribution and flow . In A. Dessler (Ed.), *Physics of the Jovian Magnetosphere*, Cambridge Planetary Science Old (pp. 395–453). Cambridge: Cambridge University Press. https://doi.org/10.1017/CBO9780511564574.013

Wilson, R. J., Bagenal, F., Delamere, P. A., Desroche, M., Fleshman, B. L., & Dols, V. (2013). Evidence from radial velocity measurements of a global electric field in saturn's inner magnetosphere. *Journal of Geophysical Research: Space Physics*, *118*, 2122–2132. https://doi.org/10.1002/jgra.50251

Wilson, R. J., Bagenal, F., & Persoon, A. M. (2017). Survey of thermal plasma ions in saturn's magnetosphere utilizing a forward model. *Journal of Geophysical Research: Space Physics*, *122*, 7256–7278. https://doi.org/10.1002/2017JA024117

Young, D. T., Berthelier, J. J., Blanc, M., Burch, J. L., Coates, A. J., Goldstein, R., et al. (2004). Cassini plasma spectrometer investigation. *Space Science Reviews*, *114*(1), 1–112. https://doi.org/10.1007/s11214-004-1406-4